PERGAMON

Chemical Engineering Science 56 (2001) 2495–2509

Chemical Engineering Science

www.elsevier.nl/locate/ces

The microscopic modelling of hydrodynamics in industrial crystallisers

A. ten Cate[a,b,c,*], J. J. Derksen[a], H. J. M. Kramer[b], G. M. van Rosmalen[b], H. E. A. Van den Akker[a]

[a]*Kramers Laboratorium voor Fysische Technologie, Delft University of Technology, Prins Bernhardlaan 6, 2628 BW Delft, The Netherlands*
[b]*Laboratory for Process Equipment, Delft University of Technology, Leeghwaterstraat 44, 2628 CA, Delft, The Netherlands*
[c]*Process Systems Engineering, DelftChemTech, Delft University of Technology, Julianalaan 136, 2628 BL, Delft, The Netherlands*

Abstract

In this contribution a method for the calculation of crystal–crystal collisions in the flow field of an industrial crystalliser is proposed. The method consists of two steps. The first step is to simulate the internal flow of the crystalliser as a whole. For this purpose, the simulation of the internal flow of an 1100 l draft tube baffled crystalliser at a Reynolds number of 240,000 is presented. This simulation was done with a lattice-Boltzmann scheme with a Smagorinsky sub-grid-scale turbulence model (c_s was 0.11) on approximately 35.5×10^6 grid nodes. The second step of the method consists of simulating individual crystals in a fully periodic box with turbulent conditions that represent the conditions in a point of the crystalliser. Thus collision frequencies and intensities of the crystals under the local hydrodynamic regime can be obtained. In this contribution a feasibility study of this second step is described. A theoretical framework is established to identify the key parameters that determine the relationship between the crystalliser flow and the box simulations. Based on this framework, conditions for box simulations representing three monitor points in the simulated crystalliser are calculated. Finally, to demonstrate the method of predicting the motion of individual particles, sedimentation and consecutive collision of a single sphere with a solid wall is simulated. © 2001 Elsevier Science Ltd. All rights reserved.

Keywords: Crystallisation; Lattice-Boltzmann; Collision rate; Large eddy simulation; Discrete particle simulation; Turbulence

1. Introduction

The design and scale-up of industrial crystallisers requires predictive models that describe the evolution of the crystal size distribution (CSD) as a function of process conditions, crystalliser layout and type of crystallisation process. Generally, these models are based on population balances, mass balances and energy balances and treat the crystalliser as a single ideally mixed vessel (MSMPR models). For evaporation crystallisation, these models generally contain strongly nonlinear kinetic expressions for crystal growth, secondary or contact nucleation and agglomeration (Gahn & Mersmann, 1999b). The model parameters are based on the volume-averaged behaviour of the entire crystalliser. However, an industrial crystalliser is far from homogeneous in terms of the physical and thermodynamic conditions. With varying crystalliser dimensions, modes of operation or types of crystalliser, these models therefore require different model parameters.

A detailed approach to modelling crystallisation processes should be able to capture the geometry of the crystalliser on the one hand and contain geometry-independent kinetic models on the other. This approach has been presented by Kramer, Bermingham, and Van Rosmalen (1999) who propose to divide the crystalliser into a number of well-defined regions in which supersaturation, rate of energy dissipation, solids concentration and CSD are more or less uniformly distributed. With such an approach, kinetic parameters for these models can be obtained from lab-scale experiments or can be estimated from simulation techniques while model simulations on industrial scale are able to predict the performance of the full-scale crystallisation process.

One of the key aspects in the (dynamic) behaviour of a crystallisation process is the role of hydrodynamics. On a macroscopic scale the hydrodynamic conditions

* Correspondence address. Laboratory Kramers Laboratorium voor Fysische Technology, Delft University of Technology, Leeghwaterstraat 44, 2628 CA, Delft, The Netherlands.

0009-2509/01/$ - see front matter © 2001 Elsevier Science Ltd. All rights reserved.
PII: S0009-2509(00)00433-4

control the crystal residence time and circulation time in the crystalliser. On a microscopic scale, key processes such as crystal collisions (source for secondary nucleation and agglomeration) and mass transfer for crystal growth are largely determined by the smallest scale flow phenomena. One of the main difficulties in correctly capturing the effect of the crystalliser hydrodynamics on the evolution of the crystal product is that the length and time scales in a crystallisation process vary widely. At one end of the spectrum there are the crystalliser length and time scales, which lie in ranges of metres and hours. At the other end, one can consider the individual crystals in the turbulent flow field. Here dominating length scales are in the range of 100–1000 μm for the crystals and 10–100 μm for the smallest fluid eddies. Time scales are of the order of milliseconds. The main question is how to integrate these widely varying scales and formulate a consistent method for estimating the influence of the small-scale phenomena on the overall performance of the crystalliser.

In this paper a method is proposed to solve part of the above posed question. The crystal–crystal collision rate is an important parameter in describing both agglomeration and the formation of attrition fragments and thus plays an important role in the crystalliser behaviour. The crystal motion is directly related to the local hydrodynamic conditions. Therefore, a relationship between the macroscopic and microscopic hydrodynamic conditions needs to be established to predict collision rates in the crystalliser accurately. In this contribution, a two-step method is proposed.

The first step of our method is to perform computational fluid dynamics (CFD) simulations of a given crystallisation process. From these simulations, characteristic flow data are obtained that describe the local hydrodynamic conditions of the crystalliser. The fluid phase (typically containing 10–20 vol% solids) is treated as a single phase with a homogeneous density and viscosity, characteristic for the crystal slurry. This approach limits the method. It can only be applied to simulations of crystalliser flow with a virtually homogeneous slurry concentration, i.e. to crystallisers at lab to pilot scale at high Reynolds numbers. This assumption can be relieved by taking into account the particle transport, for instance by solving a particle dispersion equation (e.g. Liu, 1999) and coupling back of the particle concentration to a sub-grid-scale model that locally modifies the fluid viscosity, comparable to sub-grid-scale turbulence modelling. Typical parameters that are obtained from these simulations are rates of energy dissipation, turbulent kinetic energy and fluid velocity. These parameters are obtained at the resolution of the CFD simulation, which is at least one order of magnitude larger than the particle size of the crystallisation process.

The second step of our method is to focus on the individual crystals in the crystalliser. A transition is made from a pseudo-single-phase simulation to an explicit two-phase simulation and thus, a transition is made from crystalliser flow simulations to highly detailed CFD simulations of individually suspended particles (see Fig. 1). The simulated particles are implemented at high resolution with respect to the CFD grid and therefore typically occupy a number of grid nodes. The crystalliser slurry consists of high-inertia particles (i.e. particles that do not follow the streamlines of the turbulent fluid motion) at high volume concentrations. CFD simulations of colliding particles under turbulent fluid motion are reported by, for instance, Sundaram and Collins (1997) and Chen, Kontomaris, and McLaughlin (1998), but these systems are typically investigated at (very) low particle volume concentrations which do not require a coupling between the particle and fluid motion. At high volume concentrations, particles will continuously hinder each other. Therefore, in order to accurately simulate the particle motion, a direct coupling between the fluid motion and the particle motion is required.

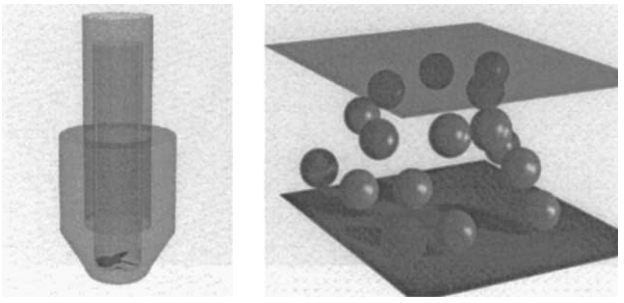

Fig. 1. Two scales of fluid motion. The macroscopic scale (crystalliser) and microscopic scale (individual particles).

The basic concept to resolve the second step is to design a box with fully periodic boundaries that contains a large number of particles. In this box turbulence is generated by forcing the fluid motion on the large scales. The turbulent flow is simulated up to the smallest occurring scales (i.e. direct numerical simulation (DNS) of the turbulent flow). The conditions in this periodic box are related to the crystalliser flow via a number of key parameters. These parameters are the turbulence characteristics obtained from the crystalliser CFD and the slurry characteristics (particle size, viscosity and density). From these so-called box simulations, the collision frequency and energy can be monitored. Collision data obtained in this way can be used in models predicting the rate of secondary nucleation and attrition (Gahn & Mersmann, 1999a) or agglomeration in crystallisers. Since the fluid phase in the crystalliser is currently assumed to be a homogeneous slurry, no back-coupling of the results from the microscopic particle simulations (e.g. streak formation of particles and turbulence modification) to the macroscopic crystalliser simulations is taken into account.

The numerical method chosen to simulate both the full-scale crystalliser flow and the suspended particles is the lattice-Boltzmann method. This method is chosen because it has a number of favourable properties. First, the method is efficient and numerically stable. Second, it has an excellent performance on parallel computers. This is an important feature, because both the equipment flow simulations and the discrete particle simulations require large computational resources. Third, the method is inherently time dependent, which makes it suitable for the implementation of a sub-grid-scale (SGS) turbulence model for large eddy simulations (LES). Turbulence modelling is required for simulation of the highly turbulent crystalliser flow. Fourth, the method can treat arbitrarily shaped boundaries which makes it suited for simulating fluid flow in irregular-shaped geometries such as a crystalliser or a cluster of moving particles. Simulations of generated isotropic turbulence are frequently done with spectral methods. Turbulence in the lattice-Boltzmann schemes can be generated by agitating the fluid at varying time and length scales with fluctuating force fields. In Section 2 the background of the lattice-Boltzmann method is discussed along with the implementation of the LES model and the treatment of the boundary conditions.

The main objective of this contribution is to establish the relationship between the two steps of the simulation methodology and to investigate the feasibility of the proposed method. For the first step, in Section 3, the CFD simulation of a pilot scale 1100 l draft tube baffled crystalliser is reported and results are presented. Then, in Section 4 an analysis is given of the hydrodynamic length and time scales that occur in the turbulent crystalliser flow and that characterise the crystalliser flow at the microscopic scale. These parameters are then used to explain how to calculate the parameters that set the scene for a representative box simulation. It is shown what the requirements of box simulations that represent three chosen monitor points in the crystalliser will be with respect to computational parameters such as the domain size and computational time for a given particle size. The box simulations are currently still under construction and therefore no results of these simulations are reported here. However, as a first example of a detailed suspended particle simulation, the lattice-Boltzmann simulation of a single particle settling towards and colliding with a solid wall is presented in Section 5. In Section 6 conclusions are drawn regarding the obtained framework.

2. The lattice-Boltzmann method

The lattice-Boltzmann method has been developed during the last decade and stems from the lattice gas cellular automata techniques that date back to the 1970s and 1980s. The concept of the lattice-Boltzmann method is based on the premise that the mesoscopic (continuum) behaviour of a fluid is determined by the behaviour of the individual molecules at the microscopic level. In the lattice-Boltzmann approach, the fluid is represented by fluid mass placed on the nodes of an equidistant grid (lattice). At each time cycle, a number of steps are executed; from each grid node, fluid mass moves to the surrounding grid nodes and conversely mass arrives at each grid node. In this way conservation of mass is guaranteed. Arriving mass collides, while collision rules are applied that guarantee conservation of momentum. After the collision step, the mass is redistributed and a cycle is finished. One of the elegant features of the method is that although the collision rules describe the fluid behaviour locally on a grid node, the continuity equation and incompressible Navier–Stokes equations are recovered (Rothman & Zaleski, 1997; Chen & Doolen, 1998). A number of recent developments in the application of the lattice-Boltzmann method clearly demonstrate its versatility. In this contribution a methodology is presented to simulate turbulent slurry flow while resolving the complete hydrodynamic environment of the particles. The first publications in which this approach to slurry flow is described are from Ladd, who applied the method to simulate slurry flow at the most detailed level (Ladd, 1994a,b) and calculated sedimentation with up to 32,000 individual particles (Ladd, 1997). Another contribution in this field is given by Heemels (1999). Multi-phase problems have also been addressed by Rothman and Zaleski (1997) (liquid–liquid) or by Sankaranarayanan, Shan, Kevrekidis, and Sundaresan (1999) (liquid–gas). Examples of lattice-Boltzmann studies in which complex and dynamic geometries are combined with mass transfer are simulations of coral growth (Kaandorp, Lowe, Frenkel, & Sloot, 1996) and biofilm growth (Picioreanu, Loosdrecht, & Heijnen, 1999; Picioreanu, 1999). The internal flow of a crystalliser is highly turbulent and requires the incorporation of an SGS turbulence model. Examples in which the method is used to investigate the turbulent fluid flow in a stirred tank are given by Eggels (1996) and Derksen and Van den Akker (1999). A review on the lattice-Boltzmann method is found in Chen and Doolen (1998).

2.1. The lattice-Boltzmann equation

Although different types of lattice-Boltzmann schemes have been developed, the different methods all stem from the evaluation of the same lattice-Boltzmann equation (LBE):

$$f_i(\mathbf{x} + \mathbf{c}_i, t + 1) = f_i(\mathbf{x}, t) + \Omega_i(f_i(\mathbf{x}, t)). \quad (1)$$

This equation states that at a position $\mathbf{x}$ and time t, an amount Ω_i is added to f_i and transported to the position $\mathbf{x} + \mathbf{c}_i$ at time $t + 1$. The subscript indicator i represents the direction of propagation and is determined by the

type of grid, $\mathbf{c}_i$ is the discrete velocity at which mass travels from one node to the other, Ω_i is the collision operator which determines the post-collision distribution of mass over the M directions on a grid node. The mass density function f_i and the collision operator Ω_i have the following universal properties:

- summation of f_i over the M directions of the chosen lattice gives the fluid density at position $\mathbf{x}$ and summation of $f_i\mathbf{c}_i$ gives the momentum vector:

$$\sum_{i=1}^{M} f_i(\mathbf{x},t) = \rho, \tag{2}$$

$$\sum_{i=1}^{M} f_i(\mathbf{x},t)\mathbf{c}_i = \rho\mathbf{u}, \tag{3}$$

- conservation of mass and momentum is guaranteed by the following equations:

$$\sum_{i=1}^{M} \Omega_i(\mathbf{x},t) = 0, \tag{4}$$

$$\sum_{i=1}^{M} \Omega\mathbf{c}_i = \mathbf{f}(\mathbf{x},t). \tag{5}$$

For the two applications discussed in this paper, two different schemes for solution of the LBE equation were used. The simulation of the internal flow of an 1100 l DTB crystalliser is based on the method of Somers (1993). Based on this method, a 3D code for LES was developed by Derksen and Van den Akker (1999). For the simulation of settling particles, a single relaxation time scheme is used (Qian, d'Humieres, & Lallemand, 1992). Both schemes obtain the same continuity equation

$$\partial_t\rho + \nabla\cdot\rho\mathbf{u} = 0 \tag{6}$$

and momentum equation

$$\partial_t\rho\mathbf{u} + \nabla\cdot\rho\mathbf{u}\mathbf{u} = -\nabla P + \nabla\cdot\nu[\nabla(\rho\mathbf{u}) + (\nabla(\rho\mathbf{u}))^{\mathrm{T}}] + \mathbf{f}. \tag{7}$$

In the compressible limit (i.e. $|\mathbf{u}| \ll u_s$) Eq. (7) corresponds to the incompressible Navier–Stokes equation. The lattice-Boltzmann method is inherently dimensionless. Length scales are treated as lattice units (equal to the grid spacing Δ) and time is represented in time steps.

2.2. Large eddy simulation

For the simulation of flows at industrially relevant Reynolds numbers (i.e. at turbulent conditions) direct simulation of the flow is not feasible and turbulence modelling is required. The time-dependent character of the lattice-Boltzmann method makes it suitable for the implementation of an SGS model. In this way large-scale motions are explicitly solved, while all small-scale motions, typically smaller than two times the grid spacing, are filtered out. This approach is usually referred to as LES. The filtering of small-scale motion is based on the assumption that the motion of the smallest scales is isotropic in nature and that the SGS energy is dissipated via an inertial subrange that has a geometry-independent character. Thus, the turbulent flow at the SGS can be represented by an SGS eddy viscosity (ν_t). The LES model applied in this research is a standard Smagorinsky model (Smagorinsky, 1963) where the eddy viscosity is related to the local rate of deformation:

$$\nu_t = l_{\mathrm{mix}}^2\sqrt{S^2}, \tag{8}$$

where l_{mix} is the mixing length of the sub-grid motion. The rate of deformation S^2 is calculated by

$$S^2 = \frac{1}{2}\left(\frac{\partial u_\alpha}{\partial x_\beta} + \frac{\partial u_\beta}{\partial x_\alpha} - \frac{2}{3}\delta_{\alpha\beta}\nabla\cdot\mathbf{u}\right)^2 \tag{9}$$

with $\delta_{\alpha\beta}$ the Kronecker delta. The Smagorinsky constant c_s is defined as the ratio between the mixing length and the grid spacing and thus also determines the cut-off length l_f of the applied LES model (Eggels, 1994):

$$l_{\mathrm{mix}} = c_s\Delta = 0.0825 l_f. \tag{10}$$

Implementation of this LES model into the lattice-Boltzmann framework is rather straightforward, because the gradients required for the rate of deformation (Eq. (9)) are essentially contained within the method. A local total viscosity ($\nu + \nu_t$) is calculated and applied in the collision step.

2.3. Boundary conditions

Boundary conditions are imposed onto the fluid via the external force vector $\mathbf{f}(\mathbf{x},t)$ from Eq. (5). A force is applied on a grid node $\mathbf{x}$ in order to manipulate the fluid with the view of obtaining a prescribed velocity at this grid node. Thus, inlet and outlet flows can be imposed, no-slip boundaries at the surface of an object can be imposed, or the fluid can be manipulated to generate velocity fluctuations to simulate turbulent conditions. When imposing the boundary of an object not located at the position of the grid nodes, an interpolation–extrapolation scheme is used. Derksen, Kooman, and Van den Akker (1997) developed a method of adaptive force fields within the lattice-Boltzmann framework. This method, used for the Somers (1993) type lattice-Boltzmann scheme has been modified for the single relaxation time scheme that is used for the particle simulation presented in Section 5.

The force field technique is best explained by the following example. Suppose one wants to impose no-slip boundary conditions at the circle within the flow domain (see Fig. 2). The circle is defined by points located in the

computational space at the crosses on the circle. These points have a velocity that is determined by the translational and rotational velocity components of the object. A force is applied at the nodes surrounding each of these points to force the fluid to obtain a velocity related to these points. This force is determined in two steps. First, the actual fluid momentum at a point on the circle is determined by first-order Lagrange interpolation from the surrounding grid nodes. Eq. (11) and Fig. 3 demonstrate this for the one-dimensional case

$$\rho\mathbf{u}_p = (\rho\mathbf{u}_1 + \mathbf{f}_1)\cdot\gamma + (\rho\mathbf{u}_2 + \mathbf{f}_2)\cdot(\mathbf{1} - \gamma). \tag{11}$$

The force applied to the grid node in a previous step is incorporated in the interpolation to account for the effect that two points on the circle may affect the fluid at the same grid node. γ represents the fractional distance between point P and point 2. Now a force is defined at point P that opposes the difference between $\mathbf{u}_p$ and $\mathbf{u}_{\text{set}}$. Second, this force $\mathbf{f}_i$, applied on nodes 1 and 2, is calculated by extrapolation of the opposing force at point P to the grid nodes using the same linear interpolation coefficient γ. For the one-dimensional example this is given by

$$\mathbf{f}'_1 = \mathbf{f}_1 + \gamma\cdot\rho(\mathbf{u}_{\text{set}} - \mathbf{u}_p), \tag{12}$$

$$\mathbf{f}'_2 = \mathbf{f}_2 + (1-\gamma)\cdot\rho(\mathbf{u}_{\text{set}} - \mathbf{u}_p). \tag{13}$$

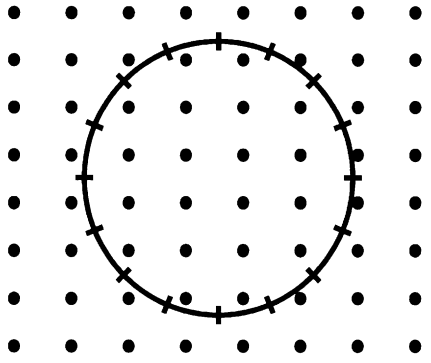

Fig. 2. Imposing a circle on a 2D lattice: (•) represent lattice nodes and (+) circle points.

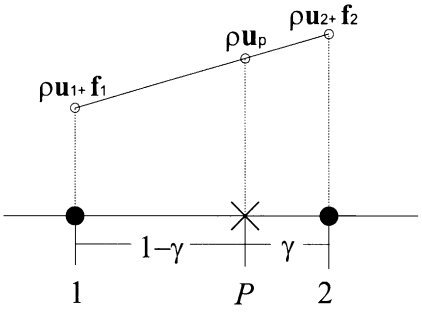

Fig. 3. Interpolation of the fluid velocity at point P between grid nodes 1 and 2.

This method can be extended to two and three dimensions by linear interpolation and extrapolation over the respective 4 or 8 surrounding nodes of an object surface point and can also be extended to higher-order interpolation schemes. The total hydrodynamic force on an object can be determined by summation of the forces applied at the grid nodes surrounding the surface of the object.

3. Crystalliser CFD simulations

As a case study, the internal flow of a pilot scale 1100 l DTB crystalliser was simulated. The crystalliser subject of this CFD study has been investigated in many previous crystallisation studies (e.g., Bermingham, Kramer, & Van Rosmalen, 1998 or Neumann, Bermingham, Kramer, & Rosmalen, 1999) for characterisation of its dynamic behaviour in crystallising ammonium sulphate and potassium nitrate under varying process conditions. Because of the complex geometry and highly turbulent operating conditions ($Re \geqslant 4\times10^5$), a high-resolution CFD simulation is required. The flow data, more specifically the turbulence characteristics, thus obtained will be used as a basis for further studies of colliding particle simulations (see Section 4).

In the following two sections, the crystalliser set-up and operating conditions are presented and the set-up of the simulation is described. Instantaneous as well as time-averaged results were obtained that are discussed in the final part of this section.

3.1. Crystalliser set-up and geometry

In Fig. 4, the crystalliser geometry and dimensions are given. The 1100 l DTB crystalliser is equipped with a marine-type impeller which is placed at the bottom section inside the draft tube.

The impeller revolves in such a way that the flow is directed upward from the bottom of the draft tube to the top section of the crystalliser. The draft tube interior contains four baffles. At the top of the crystalliser, vacuum is applied in order to lower the boiling temperature of the crystal slurry. The crystal slurry is circulated downwards along the outside of the draft tube. The outer shell of the crystalliser, equipped with six baffle skirts and six fines flow outlets, is a settling zone where an upward flow causes classification such that fine crystals are removed from the crystalliser. The flow containing fine crystals is passed through an external heat exchanger for heat input and dissolution of fine crystals and returned to the bottom section of the crystalliser. The bottom of the crystalliser also contains a feed inlet. The operating conditions of the crystalliser are given in Table 1. Under these operating conditions, the crystalliser produces ammonium sulphate crystals in the size range from 500 to 1000 μm at a slurry density of 10–20 vol%.

Table 1
Operating conditions and simulation settings of the 1100 l DTB crystalliser

Physical conditions		Simulation conditions	
Impeller speed (rpm)	320	Impeller speed (rp ts)	1/3200
v ($m^2\ s^{-1}$)	2.4×10^{-6}	v_{lB} (dimensionless)	1.4×10^{-4}
Re impeller (dimensionless)	730,000	Re impeller (dimensionless)	240,000
ϕ_v'' feed ($m\ s^{-1}$)	0.14	ϕ_v'' feed (lu/ts)	1.17×10^{-3}
ϕ_v'' fines ($m\ s^{-1}$)	1.20	ϕ_v'' fines (lu/ts)	14.6×10^{-3}
		Timestep (μs/ts)	58
		Grid spacing Δ (mm/lu)	5.0

3.2. Crystalliser simulation set-up

The crystalliser was simulated on a computational domain of $552\times253\times253$ ($\approx 35.5\times10^6$) grid nodes. Thus, a spatial resolution of 5.0 mm per lattice unit was obtained. The geometry and stirrer were implemented in the computational domain via a second-order adaptive force field technique analogous to the first-order method presented in Section 2. The Smagorinsky constant c_s was set to 0.11. In order to keep the simulation within the constraint of the compressibility limit, the impeller speed was kept well below the speed of sound of the lattice gas and was set to complete one revolution in 3200 time steps. Table 1 contains the simulation settings. The impeller Reynolds number given in Table 1 is calculated with

$$Re = \frac{ND_{\mathrm{imp}}^2}{v}. \tag{14}$$

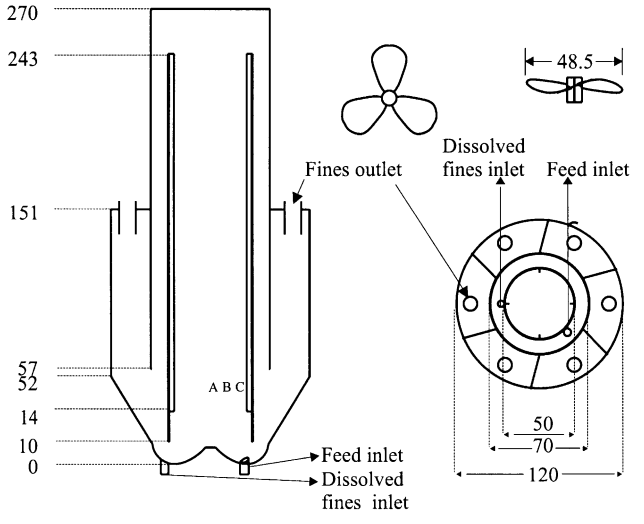

Fig. 4. Crystalliser and stirrer geometry and dimensions. Side view and top view of the 1100 l DTB crystalliser and the marine-type impeller. Dimensions are given in centimetres. The impeller is placed 12 cm from the bottom of the crystalliser. Points (A)–(C) are monitoring points, placed at (A) the centre of the crystalliser, (B) 15 cm from the centre and (C) 21 cm from the centre, 7.5 cm above the impeller in a vertical plane containing two draft tube baffles.

The impeller Reynolds number is a function of the slurry viscosity, which is a function of the slurry solids concentration. The slurry viscosity was estimated with Krieger's equation (Liu, 1999)

$$\mu = \mu_f\left(1-\frac{\phi}{\phi_{\max}}\right)^{-1.82}, \tag{15}$$

where $\phi_{\max}$ is the maximum packing limit particle concentration, which was set 0.68. The effect of the particles on the overall slurry viscosity is twofold. In the first place, during operation, the slurry density varies from 10 to 20 vol%. This causes the impeller Reynolds number to vary between approximately 400,000 and 800,000 during operation. In the second place, the slurry concentration is not homogeneously distributed throughout the crystalliser. Streaks of high and low solids concentrations will form, influencing the local viscosity throughout the crystalliser. Nevertheless, the crystalliser CFD simulation was done as a pseudo-single-phase simulation. At the given scale of 1100 l and the given high Reynolds numbers, as a first approach, the slurry density may be considered practically homogeneous. Turbulence characteristics can be scaled based on the Reynolds similarity, given that the simulation contains enough detail, which is warranted because the simulated Reynolds number is of the order of the physical Reynolds number.

The lattice-Boltzmann/LES code was parallelised by means of domain decomposition. The computational domain was divided in 8 sections. Message passing was performed by the MPI protocol. The total memory requirement for this simulation was approximately 3.0 gigabytes. The simulation was performed on 8 nodes of a parallel cluster of pentium III 500 MHz processors. The simulation of one impeller revolution on this system took about 26 h wall clock time. After development of the turbulent flow field the simulation was continued for another 6.4 impeller revolutions in order to obtain time-averaged data and time series.

3.3. Results of the crystalliser LES simulation

In Fig. 5, the velocity field and contour plot of the rate of energy dissipation are presented as found by the LES

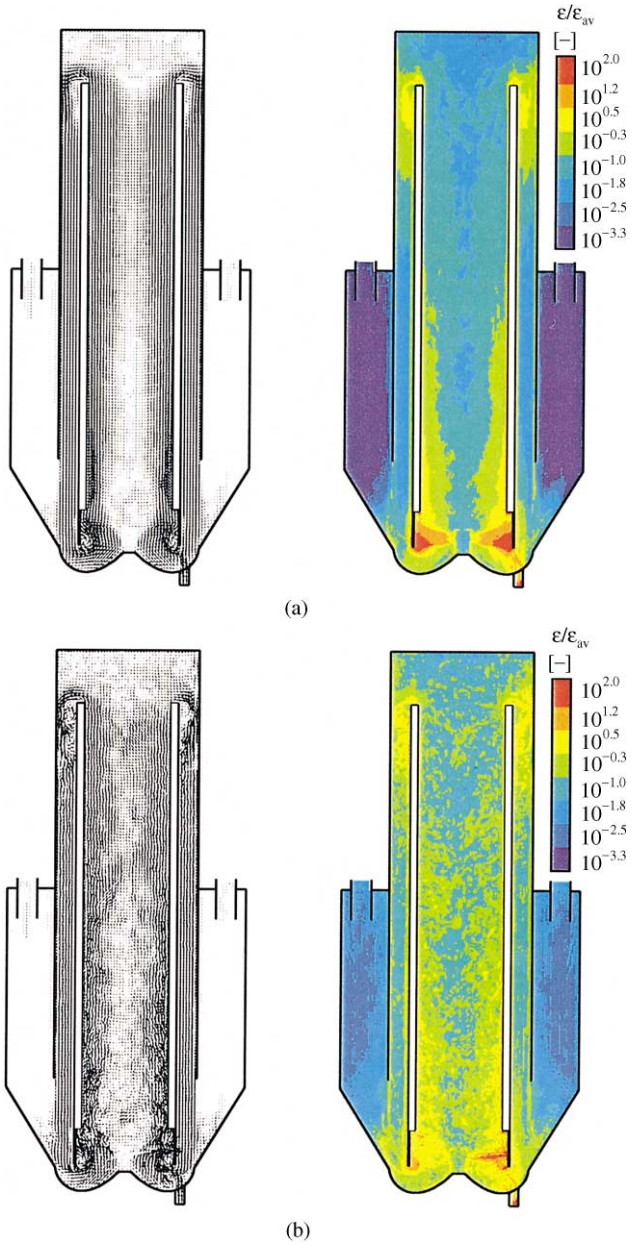

Fig. 5. Flow field of the 1100 l DTB crystalliser: (a) the time-averaged vector plot (left) and contour plot of the rate of energy dissipation (right); (b) an instantaneous realisation of vector plot (left) and contour plot of the rate of energy dissipation (right).

simulation. The time-averaged contour plot of Fig. 5(a) clearly demonstrates that a wide distribution in the rates of energy dissipation can be observed throughout the crystalliser. Of particular interest is the difference in the rate of energy dissipation between the core of the flow inside the draft tube and the outer zone. Apparently, the pumping activity of the marine-type impeller is mainly present at the impeller tip. This is observed in the vector plots of both Figs. 5(a) and (b). At a larger distance upward from the impeller, the velocity profile becomes more uniform although averaged velocities in the core

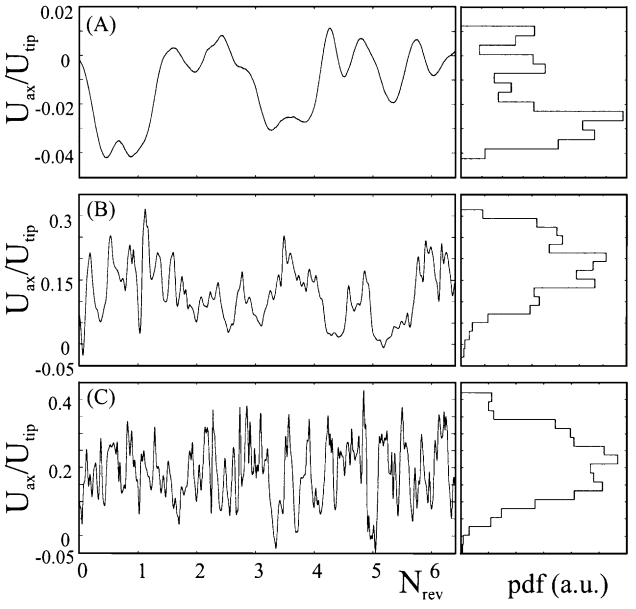

Fig. 6. Time series (left) and pdf (right) of the axial velocity component inside the draft tube at the three monitor points (A)–(C) (see Fig. 4). The p.d.f. is given in arbitrary units.

remain lower. The contour plots of the rate of energy dissipation demonstrate that energy dissipation is highest near the impeller tips and near the draft tube wall and baffles. Fig. 5(b) gives an instantaneous realisation of the flow field. In this figure the resolved turbulent structures can be clearly seen, both in the velocity field and in the rate of energy dissipation. An interesting feature is that the rate of energy dissipation in the impeller region is apparently strongly dependent on the impeller position since the contour plot of Fig. (a) gives a larger high-intensity region than that of Fig. (b).

The difference in flow characteristic at different radial positions in the crystalliser is also clearly seen in the time series of Fig. 6. At three monitor-points, (A)–(C), a time series of flow data was stored. Parameters that were determined from these points are presented in Table 3 and will be discussed more extensively in Section 4. From point (A) to (C) (from the centre to the outside of the draft tube), the frequency of the fluctuations increases, which indicates a higher degree of turbulence. A periodicity in the temporal behaviour due to the impeller passing is not observed even at this relatively close distance from the impeller. A final remark can be made about the top section of the crystalliser, where the flow enters the down-coming region. Apparently, the flow is drawn into the down comer due to the impeller action. This causes both a high degree of turbulence in the top section of the down comer and a short-circuit flow at the boiling zone.

In Table 2, the performance of the crystalliser impeller as determined from the simulations is compared to typical literature values. This table demonstrates that the

Table 2
Operating parameters from the 1100 l DTB crystalliser. Values derived from the high-resolution CFD and from literature (Neumann et al., 1999)

	From CFD	From literature
Po (dimensionless)	0.47	0.40
$\bar{\varepsilon}$ (W kg^{-1})	1.73	1.96
Pu (dimensionless)	0.30	0.32

values obtained are in the same range as those found previously in literature.

4. Length scale analysis

The objective of our study is to develop a method to predict collision rates in the turbulent flow field of an industrial crystalliser. The collision rates will be calculated from the DNS of individual particles in a periodic box. The development of the box simulations with particles is the subject of current research and is under construction (in Section 5 a single settling sphere is presented as an example of a moving particle). In this section a length and time scale analysis is made to identify the relationship between the LES simulation of the crystalliser and to explore the feasibility of a DNS-particle simulation. The LES simulations assume a pseudo-homogeneous single-phase fluid while the individual particle simulations describe a discrete two-phase system. The LES simulation is used to set the scene for the discrete particle simulations and a number of assumptions are made to identify the parameters that determine the relationship between the two types of simulations. The following two sections discuss parameters that characterise the solid phase and the turbulent crystalliser flow. The third section introduces a method to estimate the collision rate of a given type of particles in a given turbulent flow field. This collision rate is used only to estimate the required simulation time to obtain sufficient statistical data on particle collision rates. The theoretical parameters that are obtained in the following three sections are evaluated at the monitor points in the flow field of the crystalliser to demonstrate the evolving dimensions and characteristics of box simulations that represent these three points.

4.1. Parameters determined by the particulate phase

The first parameter that can be addressed is the particle size. In the type of industrial crystallisation processes subject of this work, the average particle size varies in the range of 100–1000 μm. Under the turbulent conditions of an industrial crystalliser, the Kolmogorov length scale typically ranges from 10 to 100 μm. Thus, the size of the crystals typically exceeds a number of times the Kolmogorov length scales encountered in the crystalliser. The particle diameter is obviously determined by the choice of the model system from the crystallisation process. The first approach is to represent the solid phase as monodisperse spheres with a diameter equal to the average particle size of the crystal product. The true crystal product has a CSD starting at sub-Kolmogorov length particles. Nevertheless, this choice can be justified based on the argument that the topic of interest is the collision rate and intensity. To determine attrition, only particles with sufficient inertia will fracture, being typically the larger particles. Particles are implemented at high resolution with respect to the grid spacing (see also Section 5) and therefore the particle diameter should, as a rule of thumb, cover at least 10 grid units for sufficient resolution. The grid spacing is determined by the hydrodynamic conditions (see Section 4.2) and therefore after choosing a typical particle size, the particle diameter in lattice units is fixed.

The minimum length of the box size is determined by the length at which the fluid velocities are uncorrelated (see Section 4.2). One could argue that not only the fluid velocity should be uncorrelated at half the box size, but also the particle interactions. The reason for this is that in order to prevent numerical artifacts, a particle at the centre of the box should not influence its own trajectory via the periodic boundaries of the box. Therefore, a criterion to quantify the distance at which two particles influence each other is determined by the long-range hydrodynamic interaction force. For two identical spheres in the Stokes regime, the leading term of this interaction force decays as $1/R$ (Kim & Karrila, 1991). A rule of thumb that can be applied here is that the box dimensions should exceed approximately 10–20 particle diameters for the interaction force to break down. Furthermore, because of the turbulent fluid field and the expected non-Stokesian regime of the particles, the interaction force will break down stronger than $1/R$. Thus, the criterion for the box size determined by the demand of uncorrelated turbulent flow will be strict enough to prevent the particles to be self-correlated.

The particle concentration in the box simulations is a set parameter that is chosen based on the crystal slurry concentration encountered in the crystallisation process under consideration. The main assumption that has been made for the overall crystalliser flow simulation is that the slurry flow is represented as one homogeneous fluid phase. Thus, the solid phase is assumed to be homogeneously spread throughout the crystalliser. When focussing on a small section in the crystalliser a transition is made from a pseudo-single-phase simulation to an explicit two-phase simulation of fluid with suspended particles. The assumption of a homogeneous suspension is also required for the box simulations because of the limited size of the box and the lack of knowledge on the distribution

of the crystals throughout the crystalliser. This is warranted by the fully periodic boundary conditions of the box for both the fluid phase and the particulate phase. Because of the limited size of the box and the limited number of contained particles, at any position inside the box any particle will experience a practically homogeneous and constant particle concentration.

The particle inertia can be characterised with the particle relaxation time τ_p which is a measure of the response time of a particle subject to external accelerations. For Stokesian particles this relaxation time is given by

$$\tau_p = \frac{(2\rho_p + \rho_f)d_p^2}{36\mu}. \tag{16}$$

Two particles coming from two uncorrelated eddies will collide if their inertia is large enough to make them deviate from the streamlines. The relaxation time of the particles can be used as a measure to determine which turbulent scales need to be investigated. The large-scale motion of the turbulent fluid flow will cause all particles in a cluster to move simultaneously in the same direction without effective relative motion and thus the contribution of the largest scales to collisions will be small. On the other hand, the smallest scale motion (i.e. at the Kolmogorov length scale) is typically one order of magnitude smaller than the average particle size and thus the net contribution of this motion to particle collisions will also be negligible. The scales of fluid motion that contribute most to the particle collisions are probably the scales that are identified with a time scale of the same order of magnitude as the particle relaxation time.

4.2. Turbulence length and time scales

In order to have a consistent method to translate the GS and SGS turbulent fluid motion of the crystalliser to a DNS of the fluid flow in a periodic box, the assumptions that are made for LES modelling need to be investigated and the key parameters that characterise the flow conditions at both the GS and the SGS need to be determined.

As discussed in Section 2.2, the LES modelling approach is based on the assumption that the turbulent motion at the SGS is isotropic. The kinetic energy contained at the grid scale is transported via a cascade of eddies to the smallest length scale or dissipation scale where it is dissipated. The energy spectrum of the cascade of large to small eddies is assumed to behave according to the $k^{-5/3}$ law that characterises the inertial subrange (Eggels, 1994) and can be taken as (Tennekes & Lumney, 1972)

$$E(k) = \alpha_K \varepsilon^{2/3} k^{-5/3}, \tag{17}$$

where α_K is the Kolmogorov constant with an approximate value of 1.6. Thus, the SGS motion of the LES simulation is characterised by the energy that is contained at the GS and SGS and the rate at which energy is locally dissipated. From the LES simulations, the rate of energy dissipation (ε) and the energy that is contained by the motion at the GS and the SGS turbulence, E_{GS} and E_{SGS}, are calculated according to the following equations:

$$\varepsilon = \nu_t S^2, \tag{18}$$

$$E_{GS} = \tfrac{1}{2}(u'^2 + v'^2 + w'^2), \tag{19}$$

where u', v' and w' are the root-mean-square values of the x, y and z components of the resolved velocity fluctuations. Finally, an equation for E_{SGS} (Eggels, 1994)

$$E_{\mathrm{SGS}} = \frac{\nu_t^2}{0.27 l_{\mathrm{mix}}^2} = \frac{l_{\mathrm{mix}}^2 S^2}{0.27}. \tag{20}$$

The total turbulent kinetic energy κ is given by

$$\kappa = E_{GS} + E_{\mathrm{SGS}}. \tag{21}$$

A mean square velocity related to the kinetic energy of a scale i can be calculated with

$$\overline{U_i^2} \equiv \tfrac{2}{3} E_i. \tag{22}$$

From the LES simulations a number of characteristic length and time scales can be determined that need to be resolved by the temporal and spatial resolution of a DNS of the turbulent flow. The dissipation scale or Kolmogorov length scale is the smallest length scale encountered in the turbulent flow. This length scale and the time scale associated with this length scale are given by

$$\eta = \left(\frac{\nu^3}{\varepsilon}\right)^{1/4}, \tag{23}$$

$$\tau_k = \left(\frac{\nu}{\varepsilon}\right)^{1/2}. \tag{24}$$

A criterion for good representation of the microscopic length scales is given by the demand that the grid spacing wave number times the occurring Kolmogorov length is greater than unity, i.e. the grid spacing is at approximately less than six times the Kolmogorov length (Sundaram & Collins, 1997).

A criterion that should be satisfied and determines a minimum box dimension is that the fluid velocities are uncorrelated over a distance of at least half the box length. With the assumption of the existence of an inertial subrange, the correlation coefficient $f_{11}(r)$ can be used to estimate this length. This coefficient describes the correlation of fluid velocities along a line joining two points and for the inertial subrange is given by the following equation (Abrahamson, 1975):

$$f_{11}(r) = 1 - \frac{0.9\varepsilon^{2/3} r^{2/3}}{\overline{U_i^2}}. \tag{25}$$

From this equation, the minimum distance l_0 at which velocities are uncorrelated is given when $f_{11}(r) = 0$:

$$l_0 = \frac{1.2(\overline{U_i^2})^{3/2}}{\varepsilon}. \tag{26}$$

A characteristic integral time scale is given by the eddy turnover time. This time scale is given by the ratio of the kinetic energy of turbulent motion and the rate of energy dissipation:

$$T_e = \frac{\kappa}{\varepsilon}. \tag{27}$$

An integral time scale for the SGS motion is determined by the dissipation of the SGS energy E_{SGS}:

$$T_{\mathrm{SGS}} = \frac{E_{\mathrm{SGS}}}{\varepsilon}. \tag{28}$$

4.3. Collision frequencies

In order to obtain sufficient collision statistics a (large) number of collisions must be obtained during the simulation and this sets a minimum requirement to the simulation time. Thus, to address the feasibility of the proposed simulation approach, an estimate of the collision rate is required. The theoretical framework of Abrahamson (1975) can be used to estimate collision frequencies for given particle and flow conditions. Based on kinetic gas theory, Abrahamson derived an expression for the collision rate for particles with large inertia in isotropic turbulence, which is also the subject of this study. His analysis was based on the correlation between fluid and particle motions for particles in turbulent fluid in an inertial subrange that is described by the correlation function in Eq. (25). The mean square velocity of an individual particle is calculated with (Abrahamson, 1975)

$$\frac{\overline{U_p^2}}{\overline{U_i^2}} = \frac{T_i/\tau_p + b^2}{T_i/\tau_p + 1} \tag{29}$$

and b is calculated with

$$b = \frac{3\rho_f}{(2\rho_p + \rho_f)}. \tag{30}$$

The mean square fluid velocity and time scale that need to be applied in expression (29) are estimated from either the GS or the SGS kinetic energy. The expression for the collision rate of monodisperse particles takes the form

$$Z = 4\sqrt{\pi} n_p^2 d_p^2 \sqrt{\overline{U_p^2}}. \tag{31}$$

The collision rate of Eq. (31) is used in the following section to estimate the duration of the box simulations in order to obtain sufficient collision statistics.

4.4. Length scales in the 1100 l DTB crystalliser

The data obtained from the monitor points of the crystalliser simulation are used to determine parameters of box simulations that represent the conditions at the monitor points. In Table 3, a number of properties are given.

The data presented in Table 3 clearly demonstrate an increase in turbulence towards the outside of the draft tube, as was already observed in Section 3.

In order to estimate crystal collision frequencies, a crystal system was chosen. The crystalliser of Section 3 is used to produce ammonium sulphate crystals. In Table 4 the solid and fluid phases of a typical crystal slurry are characterised. The fluid-phase properties were determined for a saturated ammonium sulphate solution.

When comparing the particle relaxation time with the time scales of the fluid motion, it is clear that the SGS energy will contribute most to the particle collisions. Thus, this energy level was used to determine the properties of a box for DNS of the SGS turbulent flow. Box dimensions are calculated based on the requirement that the Kolmogorov length scale has to be resolved (i.e. $\Delta \leqslant 0.5\eta$). The domain size (L_{box}) is set at two times the correlation length $l_{0(\mathrm{SGS})}$ (Table 5).

The compressibility requirement of the lattice-Boltzmann scheme demands that the maximum velocity is maintained well below the speed of sound. Thus, $2\bar{U}_{\mathrm{SGS}}$ was used as estimate for the maximum velocity. Due to this requirement the Kolmogorov time scale is approximately 150–200 times the temporal resolution and sufficient temporal resolution is warranted.

Table 6 gives the particle Reynolds number of the spheres. By use of Eq. (29) and (31), the collision rate that is encountered at the monitor points is determined. To obtain sufficient collisions for statistical analysis, the time

Table 3
Parameters obtained from the three monitor points

Position	ε (W kg^{-1})	E_{GS} (m^2 s^{-2})	E_{SGS} (m^2 s^{-2})	$l_{0(\mathrm{SGS})}$ (m)	η (μm)	T_e (s)	T_{SGS} (ms)	τ_k (ms)
Point (A)	0.043	0.029	0.003	0.012	133.8	1.35	66.83	7.469
Point (B)	0.959	0.285	0.020	0.010	61.61	0.59	21.26	1.582
Point (C)	4.122	0.951	0.054	0.010	42.79	0.46	13.18	0.763

Table 4
Properties of a typical ammonium sulphate slurry. The fluid properties were determined for a saturated ammonium sulphate solution at 60°C

d_p (μm) 600	n_p (# m^{-3}) 8.84×10^8
ρ_p (kg m^{-3}) 1768	ρ_f (kg m^{-3}) 1250
τ_p (ms) 24.1	μ_f (kg m^{-1} s^{-1}) 1.99×10^{-3}
C (m^3 m^{-3}) 0.10	

in which 100,000 collisions occur is taken as the simulation time. This value is given in Table 6. The last column of this table gives the number of time steps that are required for these simulations and are considered normal simulation times.

5. Sedimentation of a single particle

In this section a single settling particle is presented to demonstrate the method of the lattice-Boltzmann simulation of moving particles. A single sphere settling in a semi-periodic box is presented. A sphere that moves in a cluster of spheres under turbulent conditions will experience a continuously changing environment and will continuously collide with neighbouring particles. The simulation of a single sphere settling under gravity and colliding onto the bottom wall of a box with periodic sidewalls and rigid top and bottom wall is considered a good, first test case for the many-particle box simulations. Although the set-up appears relatively simple, a number of complex processes occur that require accurate treatment of the hydrodynamic interaction between the particle and the fluid: (1) simulation of the transient behaviour of the settling sphere requires accurate description of the flow field between the sphere and the surrounding walls and of the developing wake behind the sphere, (2) the head-on collision of the particle with the bottom wall will make the particle reverse instantaneously and requires an accurate and stable simulation technique that can treat such a discontinuity and (3) upon collision, the particle will reverse in direction and move through its own wake. The relatively simple set-up of a single settling particle in a box makes this test case also a good option for experimental validation. A recent paper on experiments of settling and collision of a sphere in a closed box is given by Gondret, Hallouin, Lance, and Petit (1999).

5.1. Set-up of the single-particle simulation

The simulation of the single settling particle was done with a single relaxation time lattice-Boltzmann scheme (Chen & Doolen, 1998). For the implementation of the no-slip boundary condition of the sphere surface the forcing method as described in Section 2 was used. The no-slip boundary condition of the box top and bottom was imposed by the so-called bounce-back boundary, a standard method for lattice-Boltzmann schemes to impose no-slip boundary conditions. The hydrodynamic force that dictates the motion of the sphere was obtained from the force applied on the grid nodes surrounding the sphere. The particle acceleration was obtained from the momentum balance of the sphere, which was used for integration of the particle trajectory. Integration of the trajectory was done via a leapfrog algorithm (Smit & Frenkel, 1996). The particle is described as a rigid sphere that makes a perfectly elastic collision. The simulation was done on a grid of $60 \times 20 \times 20$ grid nodes with a sphere with a radius of 5 grid nodes and was executed for 4500 time steps. The simulation took 9 min on a single pentium II 450 MHz processor.

Table 5
Estimates for the spatial and temporal resolution of the DNS simulation at the monitoring points (A)–(C)

Position	Timestep (μs)	Grid spacing Δ (μm)	v_{lB} (dimensionless)	L_{box} (mm)	V_{box} (mm^3)	$L_{box}/\Delta(=N_g)$ (#)	N_g^3 (# $\times 10^6$)
Point (A)	50.8	61	0.027	12	1800	182	6
Point (B)	8.81	31	0.022	10	1100	334	37
Point (C)	3.75	21	0.020	10	1100	487	115

Table 6
Estimation of the collision frequencies and particle properties for a DNS simulation of monodisperse solid spheres in the domain size given in Table 5

Position	d_p (l.u.)	N_p (#)	Re_p (dimensionless)	$\overline{U_p^2}$ (m^2 s^{-2})	Z (# m^{-3} s^{-1})	t_{sim} (s)	t_{sim}/T_{SGS} (#)	N_{ts} (#)
Point (A)	9	1590	9	0.005	1.50×10^{11}	0.37	5.6	7300
Point (B)	20	1000	16	0.016	2.56×10^{11}	0.36	16.8	40,500
Point (C)	28	1000	23	0.034	3.69×10^{11}	0.24	18.1	64,000

Table 7
Set-up and derived parameters of the single-particle sedimentation simulation

d_p (l.u.) 10	Re (dimensionless) 3.4
ρ_p (dimensionless) 540	Ri (dimensionless) 0.22
ρ_f (dimensionless) 10.8	St (dimensionless) 38.0
v_{lB} (dimensionless) 0.067	$U_{p,m}$ (l.u./t.s.) 2.28×10^{-2}

5.2. Results

In Table 7, the conditions of the simulation and a number of pertinent parameters are given. The dimensionless numbers governing the particle sedimentation, viz. the particle Reynolds number ($Re_p = U_{p,m} d_p / v$), Stokes number ($St_p = U_{p,m} d_p \rho_p / 9 v \rho_f$) and Richardson number ($Ri = (\rho_s - \rho_f) g d_p / \rho_s U_{p,m}^2$), are given and were calculated from the maximum particle sedimentation velocity ($U_{p,m}$).

In Fig. 7 snapshots of the sedimenting sphere are given and in Fig. 8 the sphere's trajectory is presented. Here the position h represents the distance between the bottom apex of the sphere and the bottom of the box. The flow pattern of Fig. 7 clearly shows the development of the circulation flow between the sphere and periodic sidewalls. The periodicity can also be observed by the fluid acceleration at the wall, indicated by the contour plot at $\theta = 1.14$ and further. As the sphere approaches the bottom wall, fluid is clearly squeezed out of the layer between the sphere and the bottom wall. After collision the particle velocity is reversed instantaneously, causing a wave to propagate through the fluid upwards, which is clearly visible at $\theta = 6.38$. This is caused due to the slight compressibility of the lattice-Boltzmann technique. In this figure the post-collision reversed fluid velocity profile around the sphere is also clearly visible.

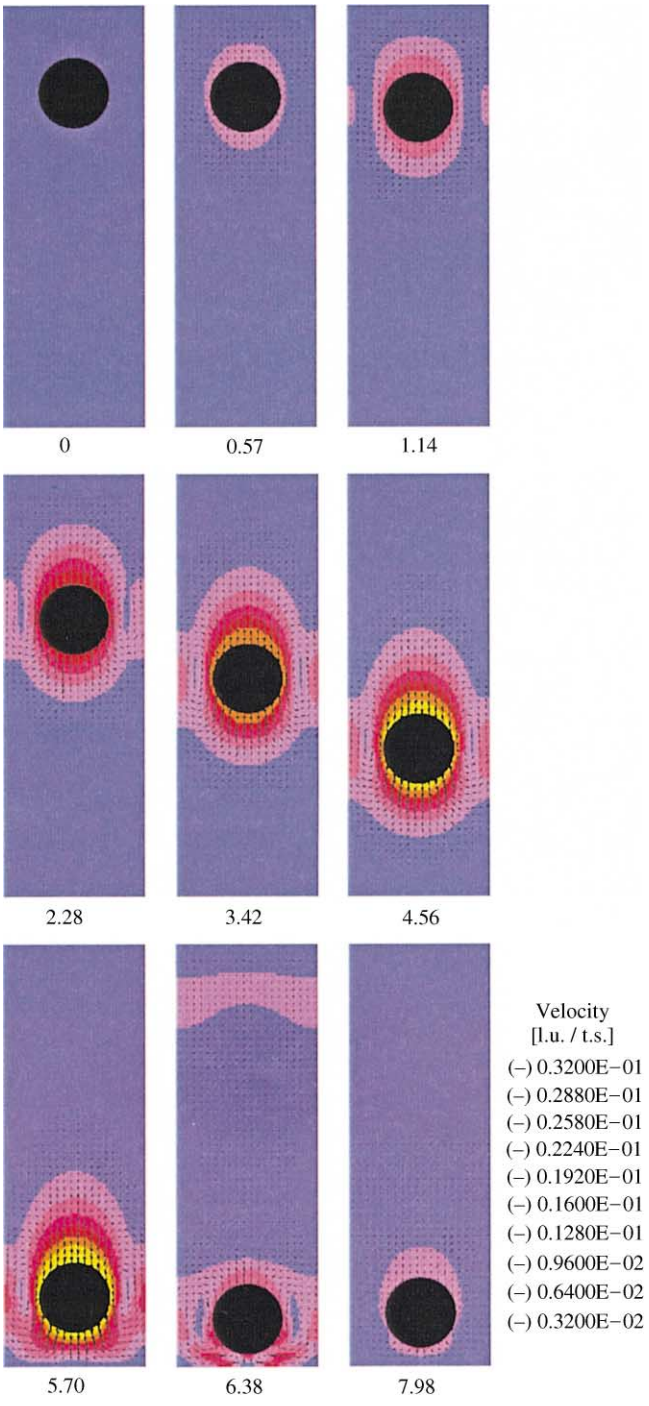

Fig. 7. Snapshots of the lattice-Boltzmann simulation of a sphere settling under a gravitational force. The contours represent the magnitude, the arrows the direction and magnitude of the fluid velocity; dimensionless velocity in lattice units per time step and dimensionless time as $\theta = t U_{p,m} / d_p$.

6. Conclusion and outlook

In this paper a methodology for the calculation of crystal–crystal collision rates in the turbulent flow field of an industrial crystalliser is presented. The collision frequency of crystals in the crystalliser is a complex function of the local hydrodynamic conditions. Therefore, accurate estimation of collision data requires knowledge of the behaviour of the flow field at the scale of the individual crystals. To obtain insight in the relationship between the overall crystalliser hydrodynamics and the motion of individual crystals in the crystalliser, the proposed method consists of simulating the internal flow of the industrial crystalliser as a whole and of simulating the motion of the individual particles suspended in the turbulent flow field in a small sub-domain (box) of the crystalliser. The flow simulations of the crystalliser as a whole can be used to set the scene for the particle simulations. Back-coupling of results from particle simulations to the crystalliser flow simulation is not considered.

It is demonstrated that the lattice-Boltzmann method combined with an LES-type turbulence model can be

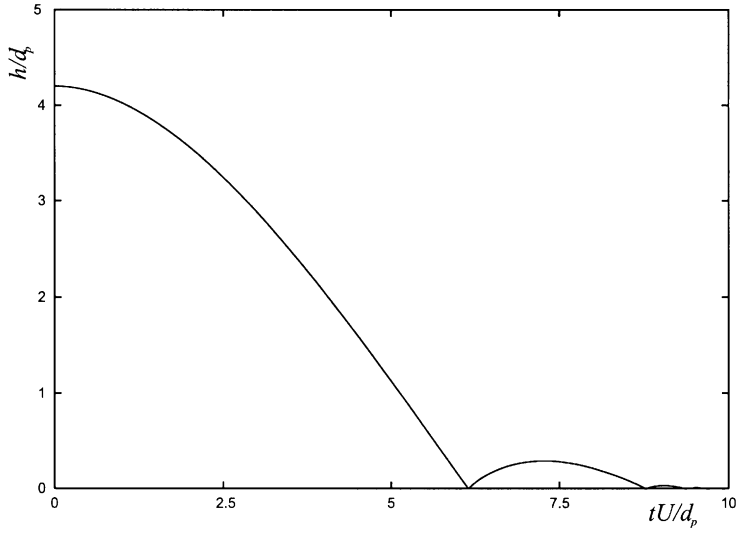

Fig. 8. The trajectory of a sphere settling under a gravitational force: dimensionless position (h/d_p) vs. dimensionless time ($\theta = tU_{p,m}/d_p$).

used as an efficient technique to resolve the complex flow field of the 1100 l DTB crystalliser. High-resolution simulations done at a Reynolds number of 240,000 produced detailed information on the turbulence characteristics of the crystalliser. A pseudo-single-phase simulation was used to represent the two-phase slurry flow of the crystalliser. Although this approach sets limitations to simulations where particle dispersion becomes an important factor for the resulting flow field, it is demonstrated that the here performed simulation is in good agreement with previous literature values for global characterising dimensionless numbers (*Po* and *Pu* numbers) of the presented crystalliser.

By analysis of the appropriate length and time scales a theoretical framework is established to relate the conditions of the crystalliser to the conditions of the box simulations. A key parameter that identifies the particle phase is the particle relaxation time, a parameter that indicates the particle response to external accelerations. Parameters obtained from the LES simulations that identify the turbulence characteristics are the turbulent kinetic energy at the GS and SGS and the rate of energy dissipation. These determine the integral time scales of fluid motion. The time scales of the same order of magnitude as the particle relaxation time will contribute most to the particle collisions. The Kolmogorov length scale of fluid motion is a measure for the smallest occurring length scales and thus dictates the spatial resolution of the box simulation. The length scale at which fluid motion is uncorrelated determines the box size. It is concluded that simulation of individual particles in a periodic box under turbulent conditions is feasible and can be used to simulate the local conditions of the crystalliser.

The many-particle box simulations are currently under development. As a first test case of microscopic particle modelling, the sedimentation and collision of a single sphere towards a solid wall is simulated to demonstrate that the lattice-Boltzmann method is capable of simulating moving and colliding spheres in a confined geometry. Special attention is required for the accurate treatment of a collision of two particles. Two approaching particles at grid-spacing distance will violate the lattice-Boltzmann framework for an accurate description of the flow in the layer between the particles which describes the evolving hydrodynamic forces. This requires a sub-grid collision model that gives an accurate treatment of the flow in the layer between the spheres. Available approaches are application of lubrication theory or the use of a collision model along the lines of a method described by Zenit and Hunt (1999). For validation of a collision model, the dynamics of a particle approaching a wall will be experimentally investigated. In our laboratory, an experimental set-up is being developed for the sedimentation and collision of a single sphere in a confined geometry. In this experiment the flow field of the sphere upon collision will be measured, using particle image velocimetry.

Future work will further consist of the application of a method to generate turbulent fluid flow in the lattice-Boltzmann framework. When this is achieved, box simulations will be performed in correspondence with the flow conditions and box dimensions estimated in this contribution. The obtained collision frequencies and intensities can be used to calculate agglomeration and attrition rates in crystallisation processes.

Notation

$\mathbf{c}_i$	discrete velocity, dimensionless
c_s	Smagorinsky constant
d_p	particle diameter, m

D_{imp}	impeller diameter, m
E	energy, $\mathrm{m^2\,s^{-2}}$
f_i	mass density function, dimensionless
f_{11}	velocity correlation function, dimensionless
$\mathbf{f}$	force vector, dimensionless
h	z-coordinate, m
k	wave number, $\mathrm{m^{-1}}$
l_{mix}	mixing length, m
l_f	cut-off length, m
l_0	zero correlation length, m
M	lattice directions, dimensionless
n_p	particle number concentration, $\#\ \mathrm{m^{-3}}$
N	impeller speed, $\mathrm{rev\,s^{-1}}$
N_p	number of particles, $\#\ \mathrm{m^{-3}}$
N_g	number of gridcells, #
N_{ts}	number of timesteps, #
P	pressure, Pa
r	distance, m
S	rate of deformation, $\mathrm{s^{-2}}$
t	time, s
T	integral time scale, s
u, v, w	velocity components, $\mathrm{m\,s^{-1}}$
u_s	speed of sound, $\mathrm{m\,s^{-1}}$
$\mathbf{u}$	velocity vector, $\mathrm{m\,s^{-1}}$
$\mathbf{x}$	position vector, dimensionless
Z	collision rate, $\#\ \mathrm{m^{-3}\,s^{-1}}$

Greek letters

Δ	grid spacing, m
$\bar{\varepsilon}$	average energy dissipation rate, $\mathrm{m^2\,s^{-3}}$
ε	energy dissipation rate, $\mathrm{m^2\,s^{-3}}$
η	Kolmogorov length scale, m
γ	length ratio, dimensionless
κ	turbulent kinetic energy, $\mathrm{m^2\,s^{-2}}$
θ	dimensionless time, dimensionless
μ	dynamic viscosity, Pa s
μ_f	dynamic viscosity of pure liquid, Pa s
ν	kinematic viscosity, $\mathrm{m^2\,s^{-1}}$
ν_t	turbulent kinematic viscosity, $\mathrm{m^2\,s^{-1}}$
ν_{lB}	kinematic viscosity of lB scheme, dimensionless
Ω_i	collision operator, dimensionless
ρ	density, $\mathrm{kg\,m^{-3}}$
τ_k	Kolmogorov time scale, s
τ_p	particle relaxation time, s
ϕ	volume fraction, dimensionless
ϕ_v''	volume flux, $\mathrm{m\,s^{-1}}$

Dimensionless numbers

Po	power number
Pu	pumping number
Re	Reynolds number
Ri	Richardson number
St	Stokes number

Acronyms

CFD	computational fluid dynamics
CSD	crystal size distribution
DNS	direct numerical simulation
DTB	draft tube baffle crystallizer
GS	grid scale
LES	large eddy simulation
SGS	sub-grid scale

References

Abrahamson, J. (1975). Collision rates of small particles in a vigorously turbulent fluid. *Chemical Engineering Science*, *30*, 1371–1379.

Bermingham, S. K., Kramer, H., & Van Rosmalen, G. M. (1998). Towards on-scale crystalliser design using compartmental models. *Computers & Chemical Engineering*, *22*, S355–S362.

Chen, M., Kontomaris, K., & McLaughlin, J. (1998). Direct numerical simulation of droplet collisions in a turbulent channel flow. Part ii: Collision rates. *Journal of Multiphase Flow*, *24*(11), 1105–1138.

Chen, S., & Doolen, G. (1998). Lattice boltzmann method for fluid flows. *Annual Review of Fluid Mechanics*, *30*, 329–364.

Derksen, J., Kooman, J., & Van den Akker, H. (1997). *Parallel fluid flow simulation by means of a lattice-boltzmann scheme*. Lecture Notes in Computer Science, vol. 1225 (p. 524). Berlin: Springer.

Derksen, J., & Van den Akker, H. (1999). Large eddy simulations on the flow driven by a rushton turbine. *A.I.Ch.E. Journal*, *45*(2), 209–221.

Eggels, J. (1994). *Direct and large Eddy simulation of turbulent flow in a cylindrical pipe geometry*. Ph.D. thesis, Laboratory for Aero- and Hydro-dynamics, Delft University of Technology, The Netherlands.

Eggels, J. (1996). Direct and large-eddy simulations of turbulent fluid flow using the lattice-boltzmann scheme. *International Journal of Heat Fluid Flow*, *17*, 307.

Gahn, C., & Mersmann, A. (1999a). Brittle fracture in crystallization processes. Part a: Attrition and abrasion of brittle solids. *Chemical Engineering Science*, *54*, 1273–1282.

Gahn, C., & Mersmann, A. (1999b). Brittle fracture in crystallization processes. Part b: Growth of fragments and scale-up of suspension crystallizers. *Chemical Engineering Science*, *54*, 1283–1292.

Gondret, P., Hallouin, E., Lance, M., & Petit, L. (1999). Experiments on the motion of a solid sphere toward a wall: From viscous dissipation to elastohydrodynamic bouncing. *Physics of Fluids*, *11*(9), 2803–2805.

Heemels, M. (1999). *Computer simulations of colloidal suspensions using an improved lattice-Boltzmann scheme*. Ph.D. thesis, Delft University of Technology.

Kaandorp, J. A., Lowe, C. P., Frenkel, D., & Sloot, P. M. A. (1996). Effect of nutrient diffusion and flow on coral morphology. *Physical Review Letters*, *77*(11), 2328–2331.

Kim, S., & Karrila, S.J. (1991). *Microhydrodynamics: Principles and selected applications.* Butterworth-Heinemann Series in Chemical Engineering. London: Butterworth-Heinemann.

Kramer, H., Bermingham, S. K., & Van Rosmalen, G. M. (1999). Design of industrial crystallisers for a required product quality. *Journal of Crystal Growth*, *198/199*, 729–737.

Ladd, A. J. (1994a). Numerical simulations of particulate suspensions via a discretized boltzmann equation. Part 1: Theoretical foundation. *Journal of Fluid Mechanics*, *271*, 285–309.

Ladd, A. J. (1994b). Numerical simulations of particulate suspensions via a discretized boltzmann equation. Part 2: Numerical results. *Journal of Fluid Mechanics*, *271*, 311–339.

Ladd, A. J. (1997). Sedimentation of homogeneous suspensions of non-brownian spheres. *Physics of Fluids*, *9*(3), 491–499.

Liu, S. (1999). Particle dispersion for suspension flow. *Chemical Engineering Science*, *54*, 873–891.

Neumann, A. M., Bermingham, S. K., Kramer, H. J., & Rosmalen, G. M., v. (1999). Modeling industrial crystallizers of different scale and type. *Proceedings of the 14th international symposium on industrial crystallization*.

Picioreanu, C. (1999). *Multidimensional modeling of biofilm structure*. Ph.D. thesis, Delft University of Technology.

Picioreanu, C., Loosdrecht, M. v., & Heijnen, J. (1999). Discrete-differential modelling of biofilm structure. *Water Science Technology*, *39*(7), 115–122.

Qian, Y., d'Humieres, D., & Lallemand, P. (1992). Lattice bgk models for navier-stokes equation. *Europhysics Letters*, *17*(6), 479–484.

Rothman, D. H., & Zaleski, S. (1997). *Lattice-gas cellular automata* (1st ed.). Cambridge: Cambridge University Press.

Sankaranarayanan, K., Shan, X., Kevrekidis, I., & Sundaresan, S. (1999). Bubble flow simulations with the lattice-boltzmann method. *Chemical Engineering Science*, *54*(21), 4817.

Smagorinsky, J. (1963). General circulation experiments with the primitive equations. 1: The basic experiment. *Monthly Weather Review*, *91*, 99–164.

Smit, B., & Frenkel, D. (1996). *Understanding molecular simulation*. New York: Academic Press.

Somers, J. (1993). Direct simulation of fluid flow with cellular automata and the lattice-boltzmann equation. *Applied Science Research*, *51*, 127–133.

Sundaram, S., & Collins, L. R. (1997). Collision statistics in an isotropic particle-laden turbulent suspension. Part 1: Direct numerical simulations. *Journal of Fluid Mechanics*, *335*, 75–109.

Tennekes, H., & Lumney, J. L. (1972). *A first course in turbulence*. Cambridge, MA: The MIT Press.

Zenit, R., & Hunt, M. L. (1999). Mechanics of immersed particle collisions. *Journal of Fluids Engineering*, *121*, 179–184.